Scientific Research Publishing

World Journal of Engineering and Technology, 2023, 11, 893-901
https://www.scirp.org/journal/wjet
ISSN Online: 2331-4249
ISSN Print: 2331-4222

On the Pre-Forging Heating Methods for AA2014 Alloy

Richard Turner, William Turner, Hao Wu

School of Metallurgy & Materials, University of Birmingham, Birmingham, UK
Email: r.p.turner@bham.ac.uk

How to cite this paper: Turner, R., Turner, W. and Wu, H. (2023) On the Pre-Forging Heating Methods for AA2014 Alloy. *World Journal of Engineering and Technology*, **11**, 893-901.
https://doi.org/10.4236/wjet.2023.114059

Received: October 26, 2023
Accepted: November 24, 2023
Published: November 27, 2023

Abstract

The aluminium alloy AA2014 is one of the most widely used of the 2xxx series alloys, owing to its superior strength-to-weight ratio and stiffness. It is commonly forged to shape for use in aerospace parts. Three different small pilot-scale AA2014 billets were subjected to different heating operations, to physically simulate a pre-forge heating operation. The unheated sample and heated samples were then analysed for micro structural evolution and mechanical properties, to understand how the pre-forge heat treatments may vary the starting condition of the alloy before being forged. It was shown that an induction heating process has the greatest impact upon the precipitation distribution. Whilst this variation is commonly considered a negative impact, the opportunity to control the induction heating to promote preferential microstructure at specific locations within the billet may be possible.

Keywords

Precipitate, Hardness, Microstructure, Heat Treatment

1. Introduction

Aluminium forms lightweight, inexpensive alloys with a good strength-to-density ratio, leading to widespread adoption across many industries, from automotive [1] to aerospace airframe [2]. The drive to reduce weight, increase efficiency and reduce carbon emissions allows aluminium alloys to improve environmentally aware vehicular and air travel. Wrought aluminium alloys are typically stronger than cast alternatives, as they have undergone strengthening processes such as cold/hot-working and heat treatment, forming a more favourable microstructure [3], leading to improvement in expected mechanical properties. Thus, wrought alloys make up over 80% of aluminium alloy produced [3]. Wrought alloys are classified into eight series, by the primary alloying element. The 2xxx series has

copper as the primary alloying element. These wrought alloys are used in the fabrication of airframe fuselage and wing skins [4] because they match the required material strength and stiffness.

Saleh [4] studied heat treatments of AA2014 with varying soak temperatures for ageing (140˚C - 190˚C) and times (1 - 16 hr), and their impact upon the evolving microstructure. It was shown that the optimal solutionizing temperature was 513˚C. Below 503˚C, there was a trend for increasing hardness with increasing soak-time. Microstructural variations throughout ageing treatments of AA2014 were evident. The existence of various phases and precipitation sequences correlated with variation in hardness. Atik [5] considered the change in yield strength of AA2014 with different ageing conditions. Through computational neural networks, fed by metallurgical-related trends regarding the formation of precipitates and their hardening effect, they were able to predict the emerging mechanical properties including yield strength, as a function of the heating parameters. From an experimental perspective, Singh [6] studied the influence of thermomechanical ageing on the mechanical properties of AA2014, showing that the strengthening effects are due to Guinier-Preston (GP) zones [7], extremely fine solute-enriched particulates, commonly referred to as θ' when precipitates are coherent, and θ when partially coherent which pin dislocations, resulting in even greater strengthening than solid solution strengthening can achieve. The precipitates are enriched in copper, which makes them commonly formed in these 2xxx alloys.

Forging companies have a range of pre-forging heating methods to soak samples at the required forging temperature. These vary depending upon billet size and quantity, and can include; induction coil, gas furnace, electric furnace or infrared heating. These will all have different heating rates and soak times associated with the process. As such, it becomes of interest to academia and industry alike to improve the current understanding of the relationship between heating methods, their impact upon microstructure, and the ensuing mechanical properties. As such, a novel research project was carried out to understand how different pre-forge heating methods may alter the billet material microstructure evolution and associated mechanical properties, which may in turn play a role in varying the emerging as-forged material and properties.

2. Material and Methods

Small pilot-scale billets of AA2014 measuring 58 mm diameter by 40 mm height were machined from a longer bar, formed via standard extrusion methods. The extrusion process will cause grain elongation in the as-extruded direction. One piece of the sectioned bar was held back as a control piece, whilst the other two pieces were subject to typical pre-forging heating routes, using induction-coil and gas-furnace methods, heated to 425˚C. Heating rates and soak times are indicated in **Table 1**. All samples were then water-quench cooled to room temperature rapidly.

Table 1. Heating soak times for the different pre-forge heating strategies.

Sample	Heating Method	Soak time (min)	Typical heating rate (˚C/min)
1	Unheated	n/a	0
2	Induction coil	4.5	120
3	Gas-furnace	60	15

The billets were first sectioned across the transverse planes to form 10 mm thick discs. Then a series of 10 mm × 10 mm × 10 mm cubes were sectioned from billets, one from the centre, and one at the outer edge, leaving the surfaces being analysed perpendicular to the extrusion direction.

The relevant faces of each cube were polished with increasing polishing grit until a colloidal silica stage leaving a mirror finish suitable for scanning electron microscopy (SEM). A TESCAN MIRA SEM was utilised for measuring grain structures using electron backscattered diffraction (EBSD) and imaging the precipitate distributions in secondary electron mode. After analysis, a series of Vickers microhardness tests were conducted across each analysed cube, using a 0.5 kg load, with a 1 mm spacing employed to prevent any overlap of associated stress fields. Miniature tensile test bars measuring 36 mm length, with a gauge length of 13 mm by 3 mm wide, and a thickness of 1.2 mm were machined from the pilot-scale billets, and were tensile tested on an Instron machine, at a deformation rate of 1 mm/min.

3. Results and Discussion

Figure 1 shows the EBSD inverse pole figures (IPF) along the extrusion direction for the unheated control sample (**Figure 1(a)**, **Figure 1(b)**), the shortest soak-time induction coil sample (**Figure 1(c)**, **Figure 1(d)**), and the longest soak-time gas-furnace sample (**Figure 1(e)**, **Figure 1(f)**) respectively. Clearly, all cross-sections exhibit a typical double fibre texture with major grains oriented along <001> (red) and <111> (blue) directions. A similar texture configuration of aluminium alloy is commonly subjected to rolling or extrusion processing which alters the grain orientations along the rolling or extrusion directions [8] [9] [10]. The {100} and {111} pole figures of the relative EBSD maps are shown in **Figure 2**.

The pole figures agree with the observations of the EBSD maps, confirming that the predominant orientation of the grains aligns with the <111> axis parallel to the direction of extrusion whilst a smaller fraction of the grains align with the <100> axis. There is no notable change in the texture that is altered by the heat treatments. In addition, the grain morphology in the central region was large and relatively random in shape, with fine recrystallised grains in between. In contrast, grains in the edge region were smaller and possessed a regular ellipsoidal shape. The SEM micrographs were analysed to determine the smaller fine-precipitated particles, as well as the coarser ones, observed within the unheated and heated AA2014 samples. **Figure 3** shows images from the unheated

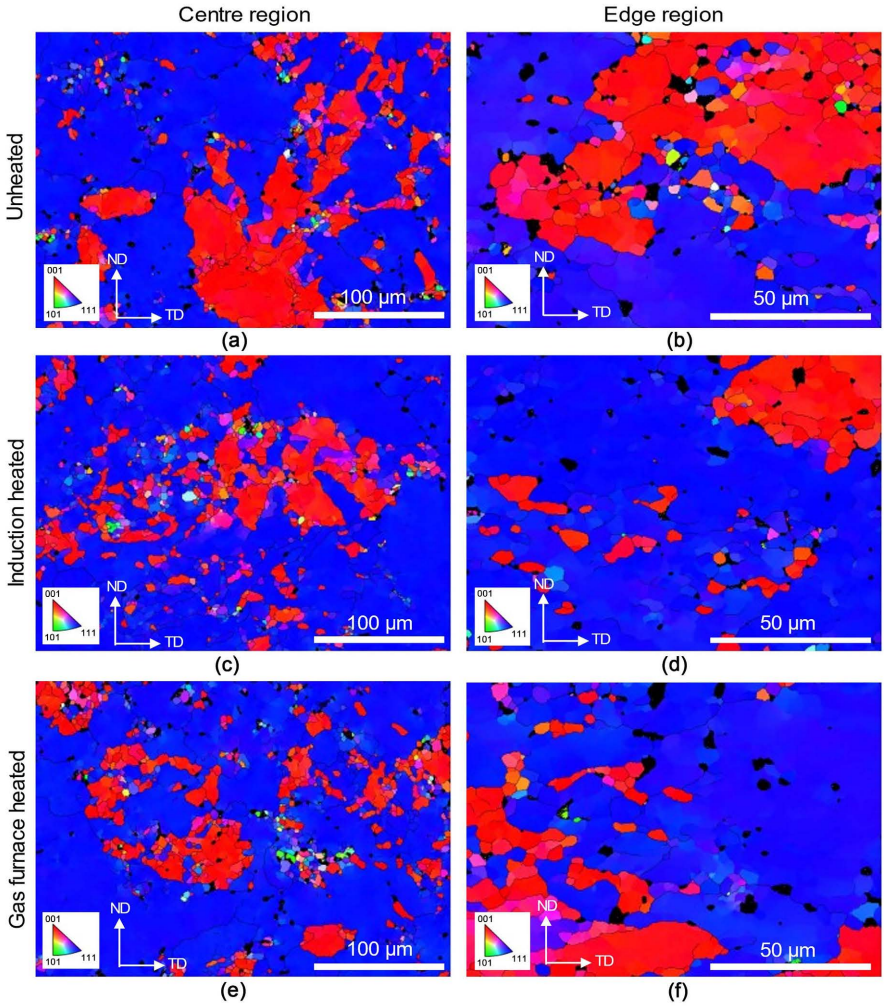

Figure 1. EBSD IPF maps (relative to the extrusion direction) of (a) (b) unheated, (c) (d) induction coil heated, and (e) (f) gas furnace heated samples taken at the centre and edge regions.

sample, as well as the induction-heated (short soak-time) sample and the gas-furnace (long soak-time) sample. The unheated sample (**Figure 3(a)**, **Figure 3(b)**) shows largely the same distribution of coarse precipitates at both central and edge regions, as no additional heating occurred. For the longer soak times but the slower heating rate of the gas furnace, it is evident that only a slight dissolution of the large precipitates occurred, compared to the unheated sample. However, for the faster heating-rate, but shorter soak time of the induction-heated sample, there is a distinct difference in precipitate distribution. Obvious dissolution of large precipitate particles occurred in both centre and edge samples compared to unheated material. Meanwhile, there is a high density of fine precipitates observed to persist in the induction-heated samples. Furthermore, there is no significant difference in precipitation distribution between the centre and edge regions for all samples.

Upon measurement, there is little grain size variation with the different heating methods and the unheated sample in both centre and edge regions, see **Figure 4(a)**.

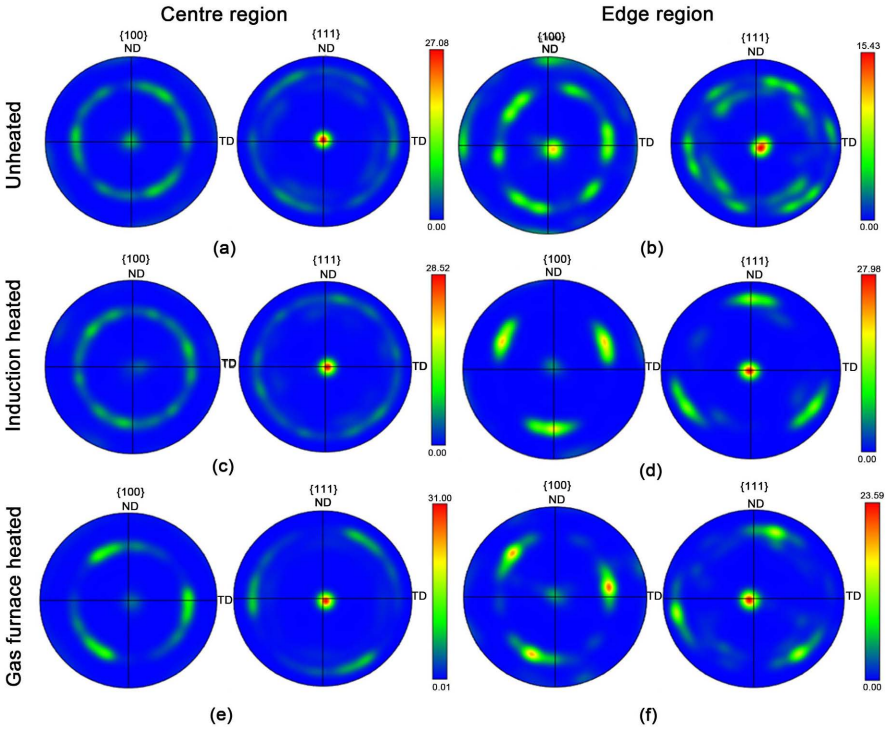

Figure 2. {100} and {111} pole figures perpendicular to the direction of extrusion of the corresponding EBSD maps in **Figure 1**.

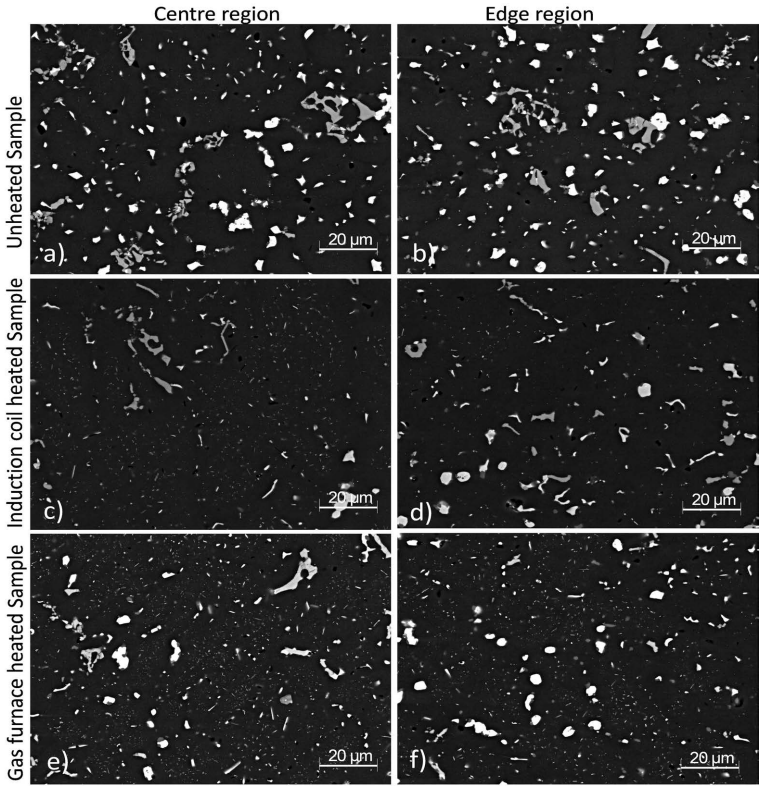

Figure 3. SEM imaging from the (a), (b) unheated, (c), (d) induction heated and (e), (f) gas furnace heated samples. Images a, c and e are from sample centre, and images b, d and f are from sample edge.

The tensile test results (**Figure 4(b)**), comparing the strength of the induction-heated and unheated samples, illustrate the marked difference upon the mechanical properties that pre-forge heating methods can have. For the hardness measurements across the samples, for unheated and gas-furnace heated samples, the edge presented a slightly higher hardness than the centre. This was particularly evident for the gas-furnace sample, whereby the outer 2 - 3 mm region displays a significant increase in measured hardness, compared to central regions (**Figure 5(a)**). This may be due to the skin effect [11] which resulted in inhomogeneous heating throughout the radius. For the induction heating method, faster heating rates produce significantly higher and more uniform hardness values throughout.

There is also a reversed hardness profile, whereby the central region is marginally harder than the edge, see **Figure 5(b)**. It is also noteworthy that natural ageing, whereby the aluminium alloy, is kept at room temperature for a prolonged period, allows for the precipitation of alloying elements, commonly Cu, out of solution [12] to yield GP (1) precipitates, is suspected to have occurred in the samples analysed in this work, thus potentially reducing the effects of the different heating methods. It is common for naturally aged aluminium alloys, over sufficient time, to become harder and possess higher tensile strength. This may account for observed similarities between samples, due to delays in testing and analysis.

The significant differences observed in the induction-heated samples are of note. For the traditional furnace-based heating method, fundamental heat transfer mechanics of heat at the surface from the atmosphere is slow. Heat transfer coefficients for metal-to-air interfaces are low [13], whereas induction-heating methods cause Eddy-current losses producing a Joule heating effect [14]. It has traditionally been considered that any process-induced variation in the AA2014 microstructure and precipitate distribution is an unwanted effect, as it adds uncertainty regarding the starting condition of the material. However, depending on the selection of induction heating electrical parameters, Eddy currents can be induced at varying depths beneath the conducting billet material surface [15], and by careful processing, the user can limit the current penetration depth at this small billet size. It therefore appears plausible to control microstructural development in small billets via induction-heating, with the different locations (edge, centre) targeted for preferential microstructure evolution and precipitation formation, to improve for geability or final component properties, accordingly. The scalability of this approach for larger billets has not been considered and likely depends upon geometrical constraints such as volume and surface area, as well as processing parameters, and the fundamental electrical equations governing the formation of Eddy currents within Joule heating [15].

Future developments regarding how pre-forging heating methods, in particular induction heating approaches, can be used to target desirable microstructure would be needed to fully explore the possibilities. This could include a wider experimental programme, using large industrial billets as opposed to pilot-scale

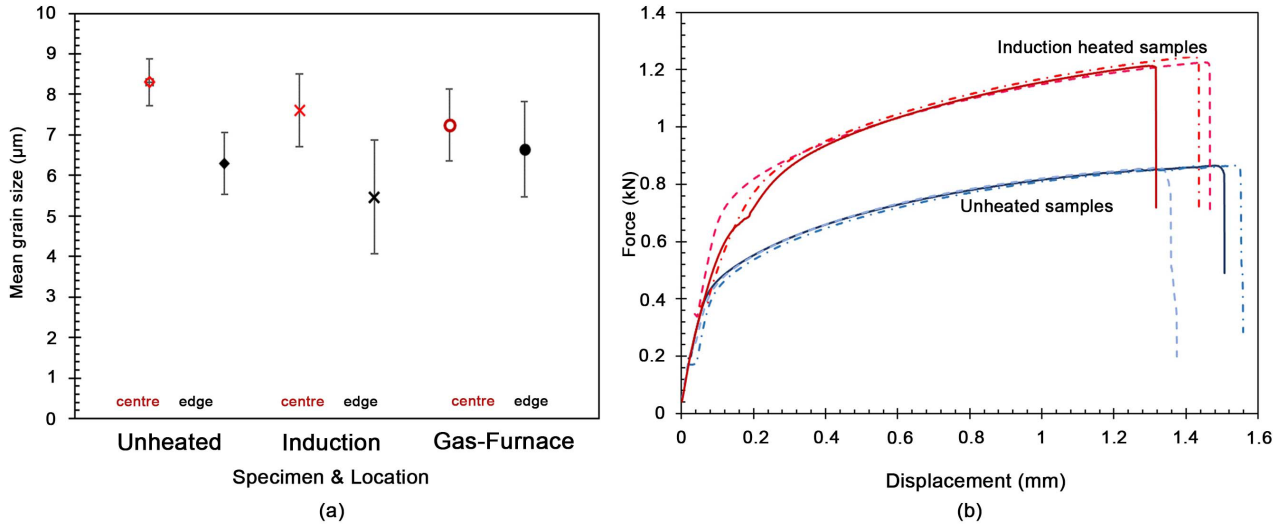

Figure 4. (a) Mean grain diameter for different locations in different heated samples, (b) Force-displacement curves for induction-heated and unheated material.

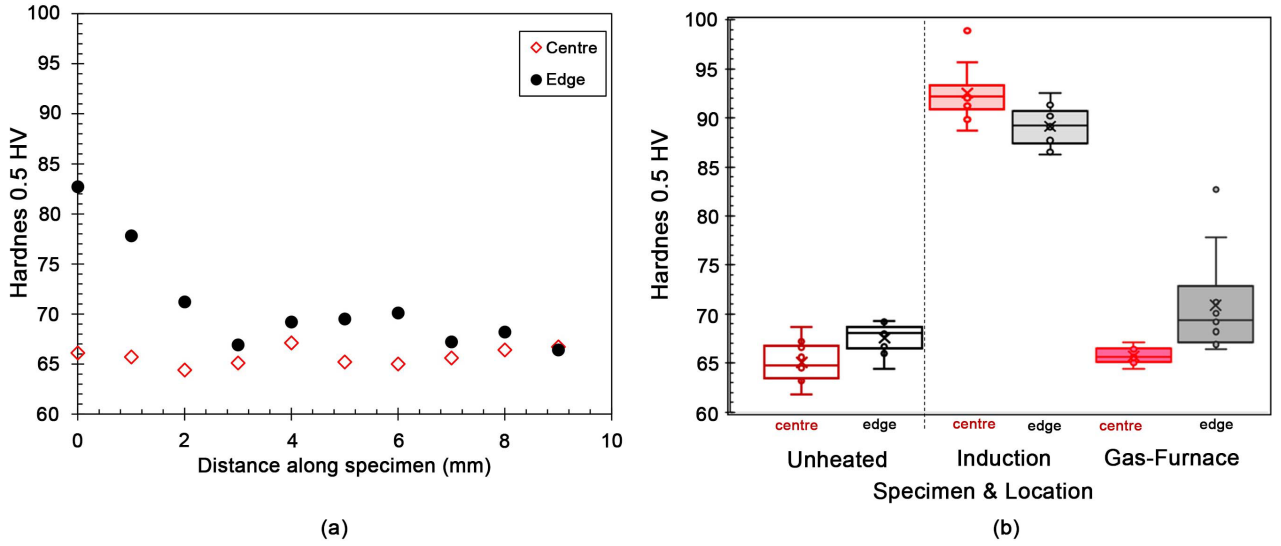

Figure 5. (a) Hardness profile across centre and edge samples for Gas-furnace heated billet; (b) Box-and-whisker distribution of Hardness measurements for analysed samples.

test pieces, a sensible design matrix of processing parameters, and potentially different alloys too. Further, thermodynamic computational models to understand grain growth effects from heating and heating rates caused by Joule heating, could be considered for a predictive capability. It is apparent however that the emerging microstructural variation at surface and core regions caused by pre-forge heating can be engineered such that this is no longer an unwanted problem for the metallurgical engineer, but instead could allow for a location-specific properties approach to optimise the in-service performance.

4. Conclusions

Three samples of AA2014 were subjected to different industrial pre-forge heat-

ing methods. These were analysed by SEM, tensile testing and hardness testing. The following conclusions are drawn.

- No significant difference in the grain structures can be observed between samples. The hardness values were independent of the variation in grain sizes.
- Traditional gas-furnace heating tends to yield a higher hardness on the outer edge of the billet compared to central, with a steeper hardness gradient along the radius.
- Induction heating, with higher heating-rate, and shorter soak time, produces an overall greater increase in hardness and mechanical strength, than slower, furnace heating methods, when compared to the unheated material.
- Induction-heating methods produce more fine precipitates at the centre of the pilot-scale billet, allowing metallurgists to target Induction settings to produce preferential microstructures pre-forging to improve material for geability, or post-forging properties.
- Future developments of pre-forging heating methods may allow for targeted location-specific properties to be incorporated into component design and the emerging microstructural evolution through processing.

Acknowledgements

The authors wish to thank Professor Yu-Lung Chiu and his Characterisation facility staff at the School of Metallurgy and Materials, University of Birmingham, and the mechanical testing staff in the same school. In particular, Dr. Feng Wang, Dr. Gokul Subramanian and Dr. Manmath Dash are greatly thanked for their support with the characterisation activities within this scientific manuscript.

Conflicts of Interest

The authors declare no conflicts of interest regarding the publication of this paper.

References

[1] Long, R.S., Boettcher, E. and Crawford, D. (2017) Current and Future Uses of Aluminum in the Automotive Industry. *JOM*, **69**, 2635-2639. https://doi.org/10.1007/s11837-017-2554-9

[2] Dorward, R.C. and Pritchett, T.R. (1988) Advanced Aluminium Alloys for Aircraft and Aerospace Applications, *Materials & Design*, **9**, 63-69. https://doi.org/10.1016/0261-3069(88)90076-3

[3] Polmear, I.J. (2017) Light Alloys—Metallurgy of the Light Metals. 5th Edition, Butterworth Heinemann, Oxford. https://doi.org/10.1016/B978-0-08-099431-4.00001-4

[4] Saleh, A.A. (2018) Effect of Heat Treatment on the Mechanical Properties of AA2014 Alloy. *Contemporary Engineering Sciences*, **11**, 3409-3419. https://doi.org/10.12988/ces.2018.87345

[5] Atik, E., Meric, C. and Karlik, B. (1996) Determination of Yield Strength of 2014

Aluminium Alloy under Aging Conditions by Means of Artificial Neural Networks Method. *Mathematical and Computational Applications*, **1**, 16-20. https://doi.org/10.3390/mca1020016

[6] Singh, S. and Goel, D.B. (1990) Influence of Thermomechanical Ageing on Tensile Properties of 2014 Aluminium Alloy. *Journal of Materials Science*, **25**, 3894-3900. https://doi.org/10.1007/BF00582456

[7] Healey, J.T. (1976) Guinier Preston Zone Evolution in 7075 Al. PhD Thesis, University of Florida, Gainesville.

[8] Chrominski, W. and Lewandowska, M. (2022) Effect of Fiber Orientation on Microstructure and Texture Evolution during the Cold-Rolling of Al-Mg-Si Alloy. *Advanced Engineering Materials*, 24, Article 2101610. https://doi.org/10.1002/adem.202101610

[9] Zhang, K., Marthinsen, K., Holmedal, B., Aukrust, T. and Segatori, A. (2018) Through Thickness Variations of Deformation Texture in Round Profile Extrusions of 6063-Type Aluminium Alloy: Experiments, FEM and Crystal Plasticity Modelling. *Materials Science and Engineering*: *A*, 272, 20-29. https://doi.org/10.1016/j.msea.2018.02.081

[10] Hidalgo-Manrique, P., Yan, S., Lin, F., Hong, Q., Kinloch, I., Chen, X., Young, R., Zhang, X. and Dai, S. (2017) Microstructure and Mechanical Behaviour of Aluminium Matrix Composites Reinforced with Graphene Oxide and Carbon Nanotubes. *Journal of Materials Science*, **52**, 13466-13477. https://doi.org/10.1007/s10853-017-1450-6

[11] Tavakoli, M.H., Karbaschi, H. and Samavat, F. (2011) Influence of Workpiece Height on the Induction Heating Process. *Mathematical and Computer Modelling*, **54**, 50-58. https://doi.org/10.1016/j.mcm.2011.01.033

[12] Miyoshi, H., Kimizuka, H., Ishii, A., *et al.* (2021) Competing Nucleation of Single/Double-Layer Guinier-Preston zones in Al-Cu Alloys. *Scientific Reports*, **11**, Article No. 4503. https://doi.org/10.1038/s41598-021-83920-8

[13] Yener, T., Yener, S.C. and Mutlu, R. (2019) Convection Coefficient Estimation of Still Air Using an Infrared Thermometer and Curve-Fitting. *Journal of Engineering Technology and Applied Sciences*, **4**, 95-103. https://doi.org/10.30931/jetas.598862

[14] Shao, Q. and Liu, Y. (2021) Joule Heating Effect on Thermal Stress for a Bi-Material Interface Crack. *International Journal of Solids and Structures*, **226-227**, Article ID: 111069. https://doi.org/10.1016/j.ijsolstr.2021.111069

[15] Fisk, M. (2014) Induction Heating. In: Hetnarski, R.B., Ed., *Encyclopedia of Thermal Stresses*, Springer, Dordrecht, 2419-2426. https://doi.org/10.1007/978-94-007-2739-7_828